P4.5 APPLICATION OF THE HYDRO-ESTIMATOR RAINFALL ALGORITHM OVER HAWAII

Robert J. Kuligowski*
NOAA/NESDIS Office of Research and Applications, Camp Springs, MD

Jung-Sun Im, J. Clay Davenport
I.M. Systems Group, Kensington, MD

Roderick A. Scofield
NOAA/NESDIS Office of Research and Applications, Camp Springs, MD

1. INTRODUCTION

The Hydro-Estimator (HE; Scofield and Kuligowski 2003) has been the operational satellite rainfall algorithm of the National Environmental Satellite, Data, and Information Service (NESDIS) since the autumn of 2000, and has been available over the continental United States to National Weather Service (NWS) forecasters via the Advanced Weather Interactive Processing System (AWIPS) since the spring of 2004. The HE uses infrared (IR) window channel (10.7-µm) brightness temperatures as the main basis for discriminating raining from non-raining areas and for estimating rainfall rates, and also uses data from numerical weather prediction models to provide additional information about moisture availability, subcloud evaporation of precipitation, impact of the thermodynamic profile on cloud heights, and orographic enhancement or reduction of rainfall.

Hawaii is an area where satellite-based rainfall information would be highly useful given the incomplete radar coverage over the state and the very rapid hydrologic response of local streams to rainfall. However, the HE was developed primarily for rainfall from deep, cold-topped convective clouds. This has greatly limited its applicability to regions like Hawaii, where complex topography and oceanic air masses often combine to produce heavy rainfall from very low (warm) cloud tops (e.g., Austin et al. 1996; Szumowski et al. 1997). This makes it necessary to develop a HE-like algorithm that is specifically tailored for Hawaii's somewhat unique relationships between cloud conditions and rainfall rates.

*Corresponding author address: Dr. Robert J. Kuligowski, E/RA2 RM 712WWBG, 5200 Auth Rd., Camp Springs, MD 20746-4304; e-mail: Bob.Kuligowski@noaa.gov.

2. DATA SETS AND METHODOLOGY

2.1 Data Sets

Data from 7 days in Hawaii in 2004 that featured heavy rain were selected for the initial recalibration work: 22-23 January, 26-28 February, and 3-4 August. For all cases the following data sets were obtained:

- GOES-10 Imager brightness temperatures (T_b's) for channels 3 (6.9 µm), 4 (10.7 µm), and 5 (12.0 µm);
- Eta model temperature (T) and water vapor mixing ratio (q_v) profiles which were used to compute stability and convective equilibrium-level temperature;
- Eta model precipitable water (PW) and relative humidity (RH);
- Eta model 925 and 850 hPa winds, which were combined with digital elevation model (DEM) data at several different resolutions to determine the vertical motion component from orographic effects;
- Hourly rain gauge data;
- Base radar reflectivity data.

Since satellite estimates of rainfall provide instantaneous rates rather than accumulations over time, radar-based rainfall rates were considered to be a more appropriate calibration data set than the rain gauge data. These rain rates were obtained by converting the radar reflectivity data to rain rates using the "tropical" Z-R relationship ($Z=250R^{1.2}$, where Z is the reflectivity and R is the rain rate in mm/h). However, there are biases in such rain rates due to effects such as uncertainties in the Z-R relationship, so the radar rain rates were adjusted using rain gauge data. A basis for adjustment was obtained by aggregating the instantaneous radar rain rates into hourly totals and then regressing the rain gauge amounts against the corresponding radar rainfall totals in log-log space to account for

any nonlinearities in the relationship between the two. This adjustment equation was then applied to the instanteous radar fields. The final steps were to aggregate these radar fields to the GOES footprint size and to use the hourly radar total N1P product to identify and remove areas of beam block.

2.2 Rain/no Rain Separation

The relationship between the value of each predictor and the occurrence of rainfall was determined by computing the conditional probability of precipitation (PoP) as a function of the value of each predictor. The threshold PoP value was then selected in order to give an unbiased result (i.e., the same number of raining pixels as observed, even if they are not in the same locations). The threshold PoP can vary from the expected value of 0.50 because of noise in the data. The relative skill of each rain/no rain predictor was then evaluated by computing the Heidke Skill Score (HSS) based on the aforementioned threshold value. The best rain/no rain predictor turned out to be $T_{10.7}$, with a PoP value of 0.52 corresponding to a temperature of 230.5 K.

Experiments were then performed using $T_{10.7}$ in combination with a number of other predictors, and using PW as a second predictor resulted in some improvement in skill—specifically, the threshold $T_{10.7}$ below which rain would occur is higher for moist environments than for dry ones (Fig. 1). However, none of the efforts to add a third predictor resulted in an improvement in skill over the $T_{10.7}$-PW combination. Therefore, over Hawaii the threshold $T_{10.7}$ below which pixels would be assigned rainfall rates was selected by linearizing the rain/no rain line in Fig. 1.

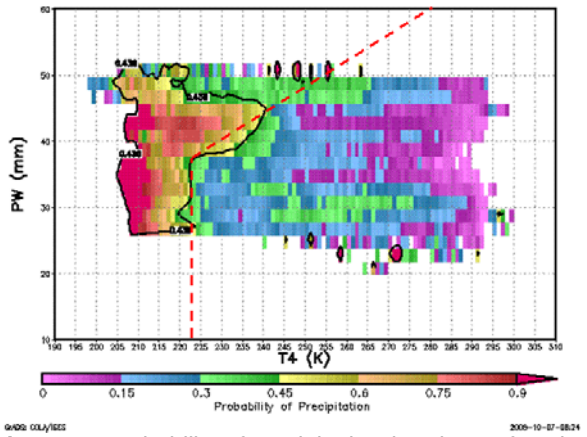

Figure 1. Probability of precipitation (PoP) as a function of both Eta model precipitable water (mm) and GOES-10 10.7-µm brightness temperature. The contour indicates the threshold value of PoP for producing an unbiased estimate of the number of raining pixels.

2.3 Rain Rate Calibration

The calibration of rainfall rate was performed using only those bias-adjusted radar pixels that were reporting nonzero rainfall. The first step was to evaluate the ability to fit each of the predictors to a function related to the rainfall rate. This was done first by plotting the rainfall rate as a function of each predictor in a Tukey box plot to get an idea of the approximate function shape (see Fig. 2a) and then by plotting the functions in log-log space to determine the best power-law fit. This

a)

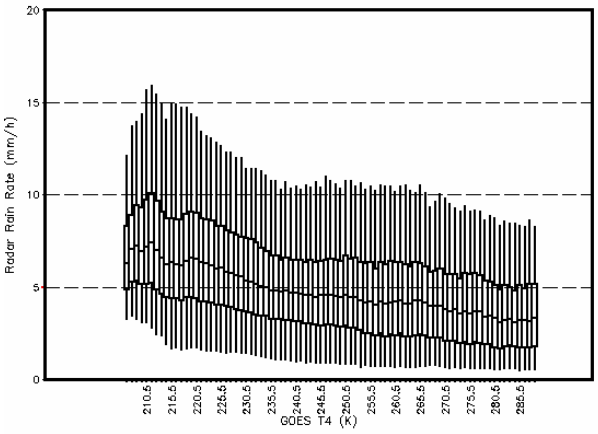

b)

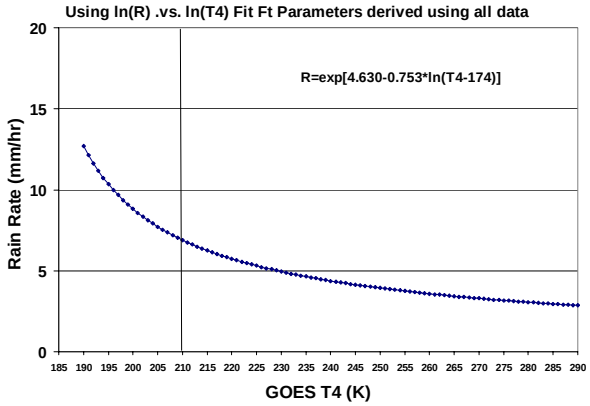

Figure 2. Relationship between T10.7 and rainfall rate over the Hawaiian Islands for the 7 days of test data, shown as (a) a Tukey box plot (box top is 75th percentile; middle is 50th percentile; bottom is 25th percentile, and whiskers extend to the 5th and 95th percentiles); and (b) a fitted function.

procedure yielded $T_{10.7}$ as the best predictor, according to the relationship shown in Fig. 2b.

Since the correlation between the rain rates derived from this equation and the observed rain rates was quite low (0.26), other predictors would be required to ensure an adequate depiction of the spatial and temporal variations in rainfall over Hawaii using the satellite data. Possible second predictors were qualitatively evaluated by dividing the data into deciles of equal size of the second predictor and looking for differences in the resulting relationships between $T_{10.7}$ and rainfall rate conditioned on the value of the second predictor. Of all of the predictors examined, the most promising was the stability parameter, consisting of the difference in potential temperature between the surface and 700 hPa. As shown in Fig. 3, the relationship between T10.7 and rainfall rate is quite sensitive to the value of this stability parameter.

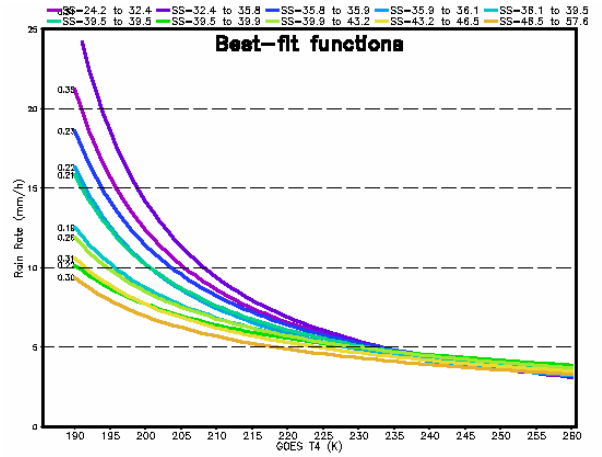

Figure 3. Rainfall rate as a function of $T_{10.7}$ for different values of stability parameter (potential temperature between the surface and 700 hPa in units of $*10^{-4}$K/m.

In order to avoid the assumption of a particular equation fit during the quantitative evaluation of the second predictor, the additive and multiplicative residuals of rain rate (i.e., estimated-observed and estimated/observed) were plotted as a function of each of the predictors to determine which predictor had the greatest value for explaining the residuals. However, none of the available predictors exhibited a significant relationship with the residuals, though some at least exhibited overall trends with a significant amount of spread. Perhaps because of this spread, the efforts to add a second predictor did not yield additional skill.

3. PRELIMINARY RESULTS

The results as of the writing of this preprint are shown in Fig. 4. The ability of the algorithm to depict the areas of most significant rainfall is quite poor in this stage of development.

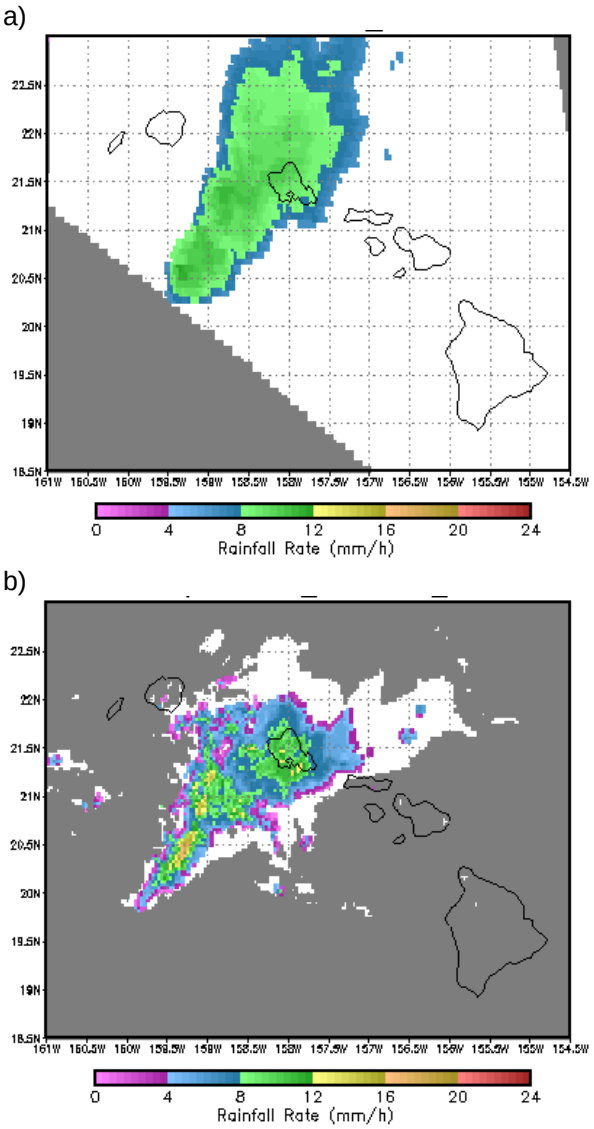

Figure 4. Comparison of preliminary satellite rainfall rates (a) with corresponding radar rain rates (b) for 1832 UTC 4 July 2004. Grey shading indicates missing data.

4. FUTURE WORK

Efforts to improve the skill of the algorithm are ongoing, including the exploration of additional predictors such as visible and near-IR satellite data during the daytime and improved orographic adjustment parameters, which were demonstrated to have little impact during the preliminary work.

5. ACKNOWLEDGMENTS

This work was partially supported by GOES Product Services Development and Improvement (G-PSDI). Radar and rain gauge data were obtained from the NOAA/NESDIS National Climatic Data Center (NCDC). GOES-10 imager data were obtained from the NOAA's Comprehensive Large Array-data Stewardship System (CLASS).

6. REFERENCES

Austin, G. R., R. M. Rauber, H. T. Ochs III, and L. J. Miller, 1996: Trade-wind clouds and Hawaiian rainbands. *Mon. Wea. Rev*. **124**, 2126-2151.

Scofield, R. A., and R. J. Kuligowski, 2003: Status and outlook of operational satellite precipitation algorithms for extreme-precipitation events. *Mon. Wea. Rev*., **18**, 1037-1051.

Szumowski, M. J., R. M. Rauber, H. T. Ochs III, and L. J. Miller, 1997: The microphysical structure and evolution of Hawaiian rainband clouds. Part I: Radar observations of rainbands containing high reflectivity cores. *J. Atmos. Sci*., **54**, 369-385.

7. DISCLAIMER